

and focal mechanisms of the aftershocks. They differ, however, in the level and extent of aftershock activity which, in the San Fernando earthquake, was at least an order of magnitude greater and was distributed through an aftershock area that was larger by a factor of 20.

A second moderate-sized earthquake ( $M_L=4.8$ ) occurred more recently within the southern frontal fault system of the Transverse Ranges province on 6 August 1973. This event, like the Point Mugu earthquake, was felt in southern California from Santa Barbara to the Los Angeles metropolitan area and beyond. The hypocenter was located 40 km west of Point Mugu and 7 km southwest of Anacapa Island, at a focal depth of 15 km. The P-wave focal mechanism solution, which is compatible with the sense of late Quaternary displacement on the Santa Cruz Island fault (13), is left-lateral strike slip movement along a fault plane striking east-west and dipping 70°S. This earthquake may have been associated with the eastern extension of that fault.

The Point Mugu and Anacapa Island earthquakes, like the San Fernando earthquake, focus attention on the likelihood that faults within the Transverse Ranges province on which movement occurred during Pleistocene time are seismically active today, and on the fact that serious seismic hazards are associated with the east-west fault systems transverse to the more widely publicized San Andreas fault system. Although the southern frontal fault system, comprised of the Malibu Coast, Santa Monica, Raymond Hill, Sierra Madre, and Cucamonga faults (Fig. 1), may not be capable of generating as large an earthquake as the San Andreas system, the frontal fault system passes directly through the Los Angeles metropolitan area and for this reason must be regarded as potentially as dangerous to the metropolitan area as the more distant San Andreas system.

W. L. ELLSWORTH, R. H. CAMPBELL  
D. P. HILL, R. A. PAGE

National Center for Earthquake  
Research, U.S. Geological Survey,  
Menlo Park, California 94025

R. W. ALEWINE, III, T. C. HANKS  
T. H. HEATON, J. A. HILEMAN  
H. KANAMORI, B. MINSTER  
J. H. WHITCOMB

Seismological Laboratory,  
California Institute of Technology,  
Pasadena 91109

#### References and Notes

1. W. F. Barbat, in *Habitat of Oil*, L. G. Weeks, Ed. (American Association of Petroleum Geologists, Tulsa, Okla., 1958), p. 62; R. H. Campbell and R. F. Yerkes, *Geol. Soc. Amer. Abstr. Program* (Cordilleran Section Meeting, 67th Annual Meeting) 3 (No. 2), 92 (1971).
2. *Natl. Oceanic Atmos. Admin. Earthquake Data Rep.* 15-73 (1973), p. 16.
3. R. A. Page, D. M. Boore, W. B. Joyner, H. W. Coulter, *U.S. Geol. Surv. Circ.* 672 (1972).
4. N. A. Haskell, *Bull. Seismol. Soc. Amer.* 54, 1181 (1964); *ibid.* 59, 865 (1969); K. Aki, *J. Geophys. Res.* 72, 1217 (1967); J. N. Brune, *ibid.* 75, 4997 (1970); J. C. Savage, *ibid.* 77, 3788 (1972).
5. An earthquake can be described by a dislocation model with the following parameters:  $A$ , the fault area;  $u$ , the average dislocation; and  $\Delta\sigma$ , the change in shear stress on the fault due to the introduction of the dislocation. The seismic moment is defined as  $M_0 = \mu Au$ , where  $\mu$  is the rigidity of the medium. Relations between the other parameters can be derived for a particular dislocation model.
6. H. Kanamori, *Eos Trans. Amer. Geophys. Union* 54, 372 (1973).
7. W. R. Thatcher and T. C. Hanks, *J. Geophys. Res.*, in press.
8. T. H. Heaton and R. W. Alewine, III, *Stanford Univ. Publ. Univ. Ser. Geol. Sci.* 13, 94 (1973).
9. C. R. Allen, M. Wyss, J. N. Brune, A. Grantz, R. E. Wallace, *U.S. Geol. Surv. Prof. Pap.* 787 (1972), p. 87.
10. The pattern of first arrival times recorded on the temporary seismograph network installed along the coast adjacent to the epicentral area by the California Institute of Technology and the U.S. Geological Survey and on sonobuoys dropped in the epicentral region by the University of California, San Diego, reported by H. Bradner and J. N. Brune [*Seismol. Soc. Amer. 68th Annu. Nat. Meet. Program Abstr.* (1973), p. 7] indicates that the suite of hypocenters may lie 2 to 5 km north of the reported location and at a focal depth 1 to 2 km shallower. The relative location of the main shock hypocenter near the northwestern edge of the aftershock zone is confirmed by the similar pattern of first arrivals at regional stations for the main shock and for a nearby aftershock, recorded on both regional and local seismographs.
11. R. H. Campbell, B. A. Blackerby, R. F. Yerkes, J. E. Schoellhamer, P. W. Birkeland, C. M. Wentworth, "Preliminary geologic map of the Point Dume quadrangle, Los Angeles County, California" [U.S. Geological Survey Open-File Map (1970)]; R. F. Yerkes and C. M. Wentworth, "Structure, quaternary history, and general geology of the Corral Canyon area, Los Angeles County, California" [U.S. Geological Survey Open-File Report (1965)]; R. F. Yerkes, R. H. Campbell, B. A. Blackerby, C. M. Wentworth, P. W. Birkeland, J. E. Schoellhamer, "Preliminary geologic map of the Malibu Beach quadrangle, Los Angeles County, California" [U.S. Geological Survey Open-File Map (1971)].
12. U.S. Geological Survey, *U.S. Geol. Surv. Prof. Pap.* 733 (1971).
13. W. W. Rand, *Calif. J. Mines Geol.* 27, 214 (1931); C. S. J. Bremner, *Santa Barbara Mus. Nat. Hist. Occas. Pap.* 1 (1932).
14. Contribution No. 2382, Division of Geological and Planetary Sciences, California Institute of Technology. Publication authorized by the Director, U.S. Geological Survey.

30 August 1973

## Premonitory Variations in S-Wave Velocity Anisotropy before Earthquakes in Nevada

*Abstract. Application of nonhydrostatic stress to rock induces velocity anisotropy, causing the S wave to split into two components traveling with somewhat different velocities. Large premonitory changes in the extent of S-wave splitting have been observed for two earthquakes in Nevada. Observations of the difference between the two S-wave velocities may provide a simple method for predicting earthquakes.*

Recent laboratory and theoretical studies have shown that the application of nonhydrostatic stress to rock containing cracks induces appreciable velocity anisotropy of S waves (1, 2). For an anisotropic medium, there are, in general, three velocities of elastic wave propagation and only in special directions do these reduce to purely compressional (P) and purely shear (S) motion. The S wave splits into two distinct components traveling with velocities that are generally different along a given direction of wave propagation.

This phenomenon has been called "acoustic double refraction" (1, 3) owing to its apparent similarity to the production of double refraction in glass by the application of stress. The separation between the two components of the S wave increases with increasing deviatoric stress. I describe here my observations of significant temporal changes in the extent of S-wave splitting

Table 1. Criteria for identifying SH, SV phases at Tonopah for events near Mina.

Phase SH	
1)	Little or no motion on the vertical instrument
2)	First motions generally west and south on the east-west and north-south instruments
3)	In-phase trace motions on the east-west and north-south instruments
Phase SV	
1)	First motions generally down, east, and south
2)	(a) Out-of-phase trace motions on the vertical and east-west instruments (b) In-phase trace motions on the vertical and north-south instruments
3)	Wave form of SV as seen on the vertical instrument similar to that of SH seen on the east-west or north-south instrument

precursory to two earthquakes in central Nevada in 1971.

Ryall and his co-workers (4) have made detailed studies of first-motion patterns of microearthquakes to determine the stress orientation and the mechanism of faulting in central Nevada. Their results show that faulting in this region is primarily related to crustal extension and that the fault movement is, in general, oblique-slip with strike-slip and normal fault components. The nodal plane solutions consistently indicate the tension axis to be nearly horizontal and approximately along the direction  $N60^{\circ}W-S60^{\circ}E$ . The strike of the compression axis is nearly along  $N30^{\circ}E$ , but its plunge angle shows considerable variation. The effect of temporal changes in tectonic stress on the S-wave velocity anisotropy is likely to be the largest along the direction of crustal extension.

Microearthquakes from central Nevada generally show two distinct com-

ponents of  $S_g$ , as seen on three-component, short-period seismograms, arriving at somewhat different times (5). These two phases have particle motions that are fairly close to SV (in the vertical plane) and SH (in the horizontal plane) and will be referred to as SV and SH for the sake of convenience. For near-horizontal wave propagation along azimuths close to the direction of extension, the SH phase arrives slightly earlier than the SV phase. On the basis of earlier work (2, 6), this can be explained by assuming that the compression axis is closer to the horizontal than to the vertical direction or that there is a larger fraction of strike-slip as compared to dip-slip fault movement. This assumption appears to be valid for several regions in central Nevada (7).

Most foreshocks and aftershocks for two events of magnitude  $M = 4.0$  and  $3.9$  with epicenters in the Slate Mountain (near Fairview Peak) and Mina

regions, respectively, were well recorded by the three-component seismographic station at Tonopah. The epicentral locations of all events considered in this study are shown in Fig. 1. The main shock in the Slate Mountain region (event 9) lay  $131 \text{ km } N37^{\circ}W$  of Tonopah, whereas the principal event (event 11) in the Mina area lay  $103 \text{ km } N78^{\circ}W$  of Tonopah. The source-to-receiver azimuthal directions of both principal events are thus within about  $20^{\circ}$  of the direction of the tension axis. Almost all epicenters lie within  $10 \text{ km}$  of the main event in either region.

The identification of an S phase on an earthquake record is generally much more difficult and ambiguous than the identification of a P phase because the S phase arrives on a trace already disturbed by waves of the P group. Another complicating factor is the phase difference between the components of ground motion produced by the effect of the free surface when the angle of incidence at the surface exceeds the critical angle of incidence (8). However, local earthquakes frequently have an easily recognizable  $S_g$  several times larger in amplitude than  $P_g$ . Moreover, the angle of incidence at the surface may not exceed the critical angle of incidence (9) so that the vertical and horizontal components of  $S_g$  arrive nearly in phase. Several criteria, such as directions of first motion based on theoretical SH, SV radiation patterns (10), matching of wave forms, and particle-motion diagrams were found to be useful in the correct identification of the two S phases. Examples of three-component seismograms of events near Mina, as recorded at Tonopah, are shown in Fig. 2, and the corresponding criteria for selecting the two S phases are listed in Table 1. The positions of the first troughs on SH, SV phases are marked by small arrows. The uppermost seismogram is for an event 9 days before the main shock and shows a separation between the two S components of about 0.3 second. This separation has increased to about 0.7 second in the second record which shows an event only 37 hours before the principal event. The third record again shows a separation of about 0.7 second. The main shock occurred on 7 December at 19:52 hours. The last record is for an event 10 days after the main event and shows a much smaller separation of only about 0.2 second.

Observed temporal changes in  $\Delta t = t_{SV} - t_{SH}$  for events near Slate Mountain are shown in Fig. 3A. It appears that

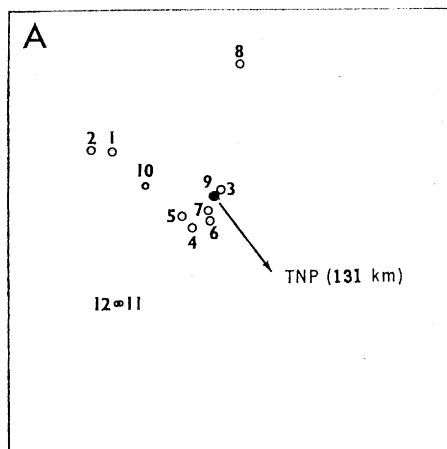


Fig. 1. Epicentral locations of (A) events 1 through 12 in the Slate Mountain region and (B) events 1 through 15 in the region near Mina. The numbers represent the chronological order of seismic events in each region. The inset map (B) shows the geographical coordinates of the two regions; TNP, MNV, and BMN represent the Tonopah, Mina, and Battle Mountain seismographic stations, respectively.

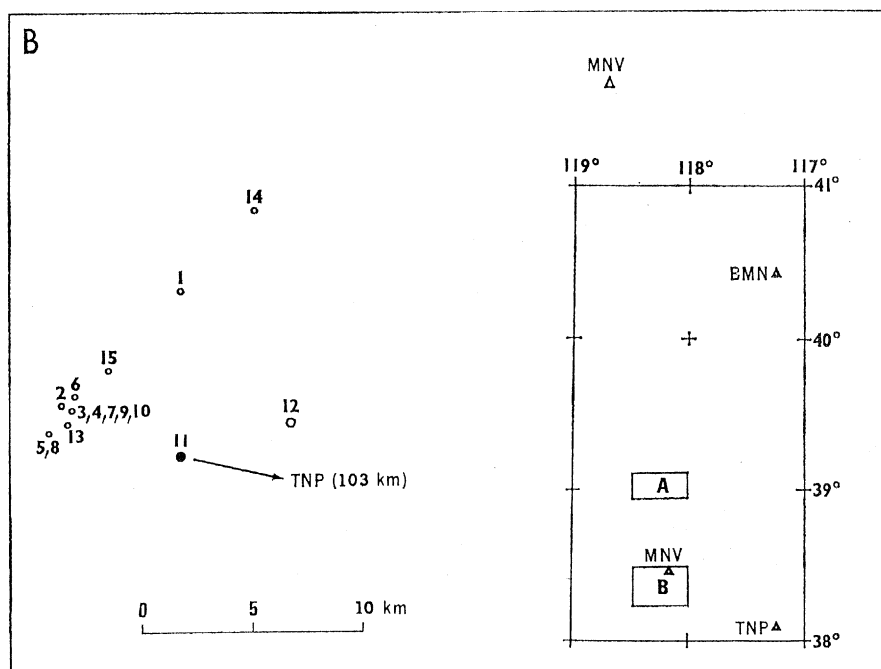


Fig. 2. Examples of three-component seismograms recorded at Tonopah from four events in the Mina region; *C*, *E*, and *N* represent the senses of the motions (namely, compression, east, and north) on the vertical, east-west, and north-south instruments, respectively.

$\Delta t$  increases gradually for the eight foreshocks, and the main shock occurs near the peak observed value of  $\Delta t$ . Results from events near Mina are shown in Fig. 3B; the main shock again takes place just after the peak observed value of  $\Delta t$ . The results here indicate a gradual return of  $\Delta t$  to its normal value after the main earthquake.

The steady increase in the observed value of  $\Delta t$  and hence in differential stress prior to an earthquake indicate pre-earthquake stress accumulation in agreement with the elastic rebound theory. Recently, a dilatancy-fluid saturation hypothesis has been proposed by several investigators (11, 12) in order to explain the premonitory changes in the ratio of S travel time to P travel time, observed in three geographically distinct regions of the world. Scholz *et al.* (13) have attempted to explain several additional premonitory phenomena on the basis of the same dilatancy-fluid flow model. The results presented here appear to be fully consistent with the dilatancy hypothesis and can be explained on its basis. Gupta (6) has studied the effect of the anisotropic properties of dilatancy on P- and S-wave velocities and suggested that pre-earthquake dilatancy should cause S-wave splitting. The value of  $\Delta t$  should be determined primarily by the degree and spatial extent of dilatancy between the source and observation point. The pre-earthquake flow of groundwater into the dilated focal region is not likely to affect  $\Delta t$  since, unlike P-wave velocity, S-wave velocity remains almost unchanged when the air in cracks is replaced by water (14). The dilatancy-fluid flow hypothesis therefore suggests that  $\Delta t$  should increase at first rather abruptly and then remain nearly constant at a high level before the earth-

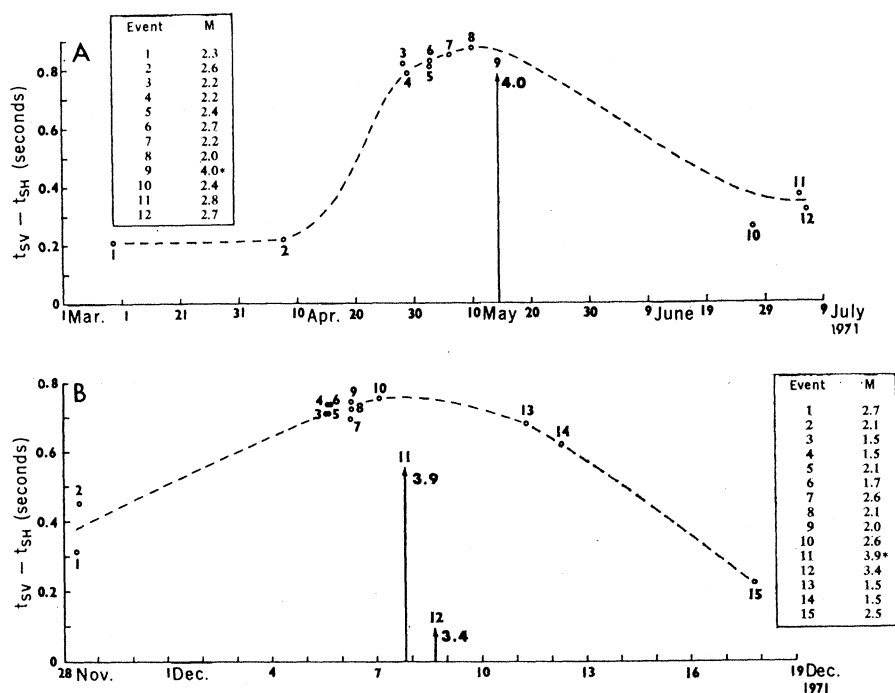
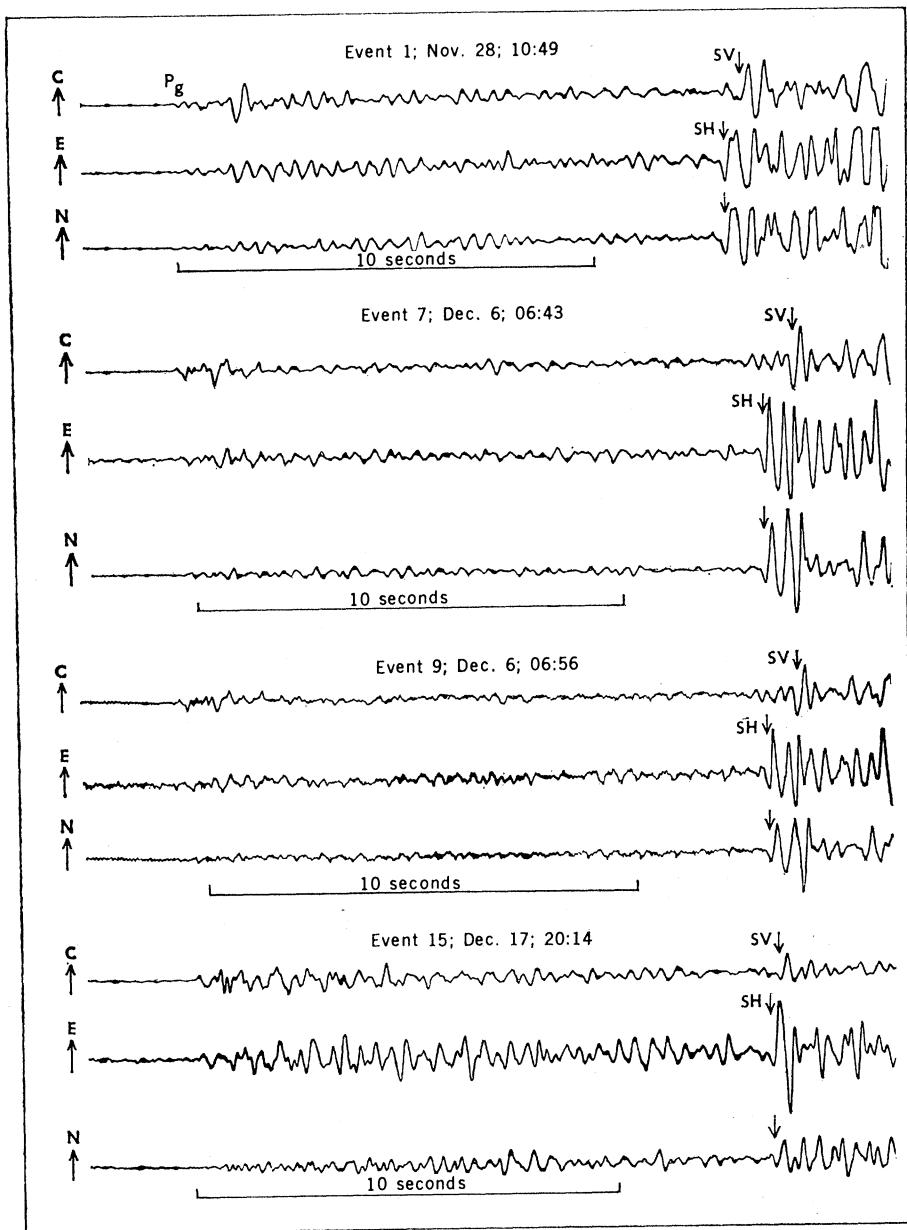


Fig. 3. Observed temporal variations in  $t_{SV} - t_{SH}$  for events in (A) the Slate Mountain region and (B) the Mina region. The maximum observed difference in the SH, SV velocities in the two regions amount to only 2.3 and 2.5 percent, respectively. The insets show magnitude (*M*) for each event. The S waves from the largest events (event 9 from the the Slate Mountain region and events 11 and 12 from the Mina region) could not be examined because of signal clipping.

quake strikes, in complete agreement with my observations. Whitcomb *et al.* (12) have examined the relationship between the precursor time interval and the magnitude of earthquakes; their results indicate a precursor time interval of about 25 days for an  $M = 4$  event. This value agrees fairly well with the duration of the premonitory episode seen in Fig. 3A. After the earthquake, the stress drop will cause the cracks to close and fluids to migrate outward. This process is likely to be relatively slow and could account for the slow return of  $\Delta t$  to its normal value.

A few seismologists have expressed the view that the observed phenomenon may be an artifact of variations in the spatial location of seismic events rather than of changes in the stress field. This possibility perhaps cannot be ruled out completely, although it is not easy to conceive a geometry giving rise to a large-amplitude SV type phase arriving a fraction of a second later than the  $S_p$  phase.

The differential stress responsible for a shallow earthquake may induce measurable pre-earthquake velocity anisotropy of the shear wave. The observed premonitory results for two earthquakes in Nevada are consistent with the elastic rebound theory and can be explained on the basis of the dilatancy-fluid saturation hypothesis. Systematic observations of the parameter  $\Delta t$  may be used to monitor stress changes, and its leveling off at a high value may signal an impending earthquake. In principle, one can monitor a given area by means of a single three-component seismograph, and the observed results are almost independent of local effects. I believe that this method has the potential for being one of the simplest ways of predicting earthquakes.

INDRA N. GUPTA

Mackay School of Mines,  
University of Nevada,  
Reno 89507

#### References and Notes

1. A. Nur and G. Simmons, *J. Geophys. Res.* **74**, 6667 (1969).
2. A. Nur, *ibid.* **76**, 2022 (1971).
3. P. Byerly, *Bull. Seismol. Soc. Amer.* **28**, 1 (1938). It is interesting to note his remark: "Perhaps the surface layers offer the phenomenon of double refraction."
4. A. Ryall and S. D. Malone, *J. Geophys. Res.* **76**, 7241 (1971); A. Ryall, B. M. Douglas, S. D. Malone, W. U. Savage, *Izv. Akad. Nauk. SSSR Fiz. Zemli.* **12**, 12 (1972).
5. I. N. Gupta, *Eos Trans. Amer. Geophys. Union* **53**, 1041 (1972).
6. ———, *Bull. Seismol. Soc. Amer.* **63**, 1157 (1973).
7. J. C. Savage and L. M. Hastie, *ibid.* **59**, 1937 (1969); F. J. Gumper and C. Scholz, *ibid.* **61**, 1413 (1971); C. M. Gilbert, M. N. Christensen, Y. Al-Rawi, K. R. Lajoie, *Geol. Soc. Amer. Mem.* **116** (1968), p. 275.
8. B. Gutenberg, *Trans. Amer. Geophys. Union*

- 33, 573 (1952); O. Nuttli, *Bull. Seismol. Soc. Amer.* **51**, 237 (1961).
9. The velocities and layer thicknesses in Nevada, based on crustal studies such as those by L. C. Pakiser and D. P. Hill [*J. Geophys. Res.* **68**, 5757 (1963)] indicate that, for an epicentral distance of about 100 km, the angle of incidence at the surface is less than the critical angle of incidence.
10. For an assumed model of faulting derived from the composite nodal plane solution of microearthquakes, one can obtain SH, SV radiation patterns using the method described by A. Ben-Menahem, S. W. Smith, T. L. Teng [*Bull. Seismol. Soc. Amer.* **55**, 203 (1965)].
11. A. Nur, *ibid.* **62**, 1217 (1972); Y. P. Aggarwal, L. R. Sykes, J. Armbruster, M. L. Sbar, *Nature* **241**, 101 (1973).
12. J. H. Whitcomb, J. D. Garmany, D. L. Anderson, *Science* **180**, 632 (1973).

13. C. H. Scholz, L. R. Sykes, Y. P. Aggarwal, *ibid.* **181**, 803 (1973).
14. A. Nur and G. Simmons, *Earth Planet. Sci. Lett.* **7**, 183 (1969).
15. This report was presented at the May 1973 meeting of the Seismological Society of America. I thank many delegates attending this meeting (especially Dr. J. H. Healy, Dr. K. Aki, Dr. M. N. Toksoz, Dr. G. E. Backus, and Y. P. Aggarwal) for useful discussions and suggestions. Sincere thanks are also due to Prof. A. Ryall for guidance and critical reading of the manuscript. Supported in part by the Advanced Research Projects Agency, monitored by the Air Force Office of Scientific Research, under contract F44620-72-C-0069 and in part by the Atomic Energy Commission under contract AT(26-1)-454.

15 June 1973; revised 1 August 1973

## Venus: Composition and Structure of the Visible Clouds

**Abstract.** *It is proposed that the visible cloud deck on Venus is composed of droplets of sulfuric acid. These are formed by the very rapid photooxidation of carbonyl sulfide in the upper atmosphere. The clouds are best described as an extensive haze since the predicted particulate scale height probably exceeds the gas scale height within the layer. The predicted mixing ratio for water is  $10^{-6}$  (lower limit), and for both carbonyl sulfide and sulfur dioxide it is  $10^{-7}$  (upper limit); these are in good agreement with observations. Gaps in the layer are not possible unless the planetary scale dynamics produce cloud turnover times of less than a few days. Under these conditions the water mixing ratio could approach  $10^{-4}$  and the formation of a thin hydrochloric acid haze at high altitude above the main cloud is possible.*

Venus is the closest planet to the earth in the solar system, and in view of the substantial literature in the field of planetary atmospheres it is surprising that there is as yet no definitive evidence on the chemical composition of the clouds which completely shroud the planet. Visual observations, together with the uniformity of the infrared emission temperatures (1), imply that there are few gaps (if any) in this cloud layer. The analysis of gaseous absorption bands (2) implies temperatures around 250°K and pressures around 200 mbar within these visible clouds. A cloud top might also be inferred around 200 mbar (altitude approximately 63 km) from the abrupt change from an adiabatic to a subadiabatic lapse rate detected at this level by Mariner 5 (3). However, a cloud top as

such is apparently difficult to define. Analyses of the degree of polarization of sunlight reflected from the planet (4) imply the existence of spherical droplets of radius about 1.1  $\mu\text{m}$  and refractive index 1.44 at the 50-mbar level, while the tenuous intermittent haze layers observed in ultraviolet photographs (5) probably lie at pressures near 10 mbar.

In view of the observation of both HCl and H<sub>2</sub>O gases on the planet, it has been suggested (6) that an upper haze layer composed of droplets of concentrated hydrochloric acid solution might be formed at temperatures around 198°K, corresponding to pressures around 20 mbar. The H<sub>2</sub>O number mixing ratio was assumed to be  $10^{-4}$  at the cloud-top level (2). However, recent observations by Fink *et al.*

Table 1. Possible reaction sequence leading to the production of H<sub>2</sub>SO<sub>4</sub> aerosols in the upper atmosphere of Venus. The constant  $J_1$  is obtained by convolving the solar ultraviolet spectrum at Venus with the COS absorption spectrum of Sidhu *et al.* (28) between 2200 and 2700 Å and dividing by 4 for a planetary average. In reactions 1 and 2, S(<sup>1</sup>D) is an excited state of sulfur.

Reaction	Rate constant	Reference
1. COS → CO + S( <sup>1</sup> D)	$J_1 = 10^{-5} \text{ sec}^{-1}$	
2. S( <sup>1</sup> D) + CO <sub>2</sub> → S + CO <sub>2</sub>	$k_2 > 1.66 \times 10^{-11} \text{ cm}^3 \text{ sec}^{-1}$	(29)
3. S + O <sub>2</sub> → SO + O	$k_3 = 2 \times 10^{-12} \text{ cm}^3 \text{ sec}^{-1}$	(30)
4. SO + OH → SO <sub>2</sub> + H	$k_4 = 1.17 \times 10^{-10} \text{ cm}^3 \text{ sec}^{-1}$	(30)
5. SO <sub>2</sub> + HO <sub>2</sub> → SO <sub>3</sub> + OH	$k_5 = 3 \times 10^{-10} \text{ cm}^3 \text{ sec}^{-1}$	(31)
6. SO <sub>3</sub> + H <sub>2</sub> O + CO <sub>2</sub> → H <sub>2</sub> SO <sub>4</sub> + CO <sub>2</sub>		